Full Paper

Propellants, Explosives, Pyrotechnics

DOI: 10.1002/prep.201900365

Ignition and Combustion Developments of Granular Explosive (RDX/HMX) in Response to Mild-Impact Loading

Yanqing Wu,*[a] Hongzheng Duan,[a] Kun Yang,[a] Hongfu Guo,[b] and Fenglei Huang[a]

Abstract: The experimental analyses of ignition and burning responses of mild-impacted granular explosive, namely, cyclotrimethylene trinitramine (RDX) and cyclotetramethylene tetranitramine (HMX), were performed based on an optimized drop-weight system equipped with a High-Speed Camera (HSC). It has been found that jetting phenomena observed by HSC is the result of the energy released by gaseous products, which push the pulverized or melted explosives to splash radially. Jetting is the only and the most obvious difference between reactive and inert particles prior to combustion so that it can be regarded as the sign of ignition more accurately than other ways. For RDX sample, the molten phase plays an important role in the hot-spots formation. After a piece of waxed paper is put on the glass anvil, the jetting of molten-phase RDX will be limited due to the high-roughness of waxed paper. Moreover, ignition growth to burning probability of RDX particles is increased compared with the non-waxed paper case. Radial deformation velocity, jetting velocity, and flame propagation velocity have been estimated via image processing, making it possible to quantify the violence of mechanical deformation and chemical reaction.

Keywords: RDX and HMX explosive · Drop-weight impact · Jetting · Ignition and combustion · Heat-generation mechanism

1 Introduction

1.1 Safety Background

Till recently, high-energy explosives such as RDX and HMX were commonly used for weaponry and rocketry applications due to their high performance [1]. However, various extreme impact conditions including low-to-medium level normal impact, projectile penetration, and needling encountering in the process of storage, transport, and weapon applications could result in unexpected catastrophic explosions of explosives [2]. Walley et al. [3] showed that impact and friction stimuli much less than those required to heat bulk explosive to the deflagration temperature could still ignite or initiate explosion by studying of accidental and intentional initiations and found that the sensitivity of explosive crystals can be reduced by (a) improving the crystal quality; (b) reducing crystal or molecular defects; (c) eliminating voids or pores; (d) eliminating chemical impurities; (e) eliminating multiple phases; (f) optimizing the particle size distribution. During the last decade, the problem of unwanted explosion of these high-energy explosives and propellants has become an issue of increasing concern [4–5].

1.2 Drop-Weight Test

The drop-weight test is the simplest and the most widely-used method of investigating breakage characteristics of inert materials [6] or assessing impact sensitivity of reactive explosives under low-velocity impact [7–9]. It contains several advantages such as flexibility, extended input energy range, and the possibility of testing particle beds [10–11]. The sensitivity of explosives is usually evaluated in terms of the H_{50} value after dropping a 2.5 kg weight from a predetermined height onto the striker plate [12–13]. Due to its convenience for assessing sensitivity, simple relationships between H_{50} and molecular properties have also been established as estimations of impact sensitivities [14–18]. Unfortunately, drop weight explosive sensitivity rankings from various laboratories do not agree well, partly due to the various 'Go' criteria used by different operators [19–21]. To overcome key limitations of the drop-weight test and obtain quantitative data of impact sensitivity, researchers have made many improvements for the drop-weight test [22–25]. Tavares [24] employed drop-weight tests to determine energy-size reduction relationships for breakage of particulate materials. They proposed a calculation method to determine the comminution energy and the coefficient of restitution in drop-weight tests. Joshi et al. [25] developed an apparatus that was a hybrid of the split Hopkinson pressure bar (SHPB) and the conventional drop-weight test. The ap-

[a] *Y. Wu, H. Duan, K. Yang, F. Huang*
State Key Laboratory of Explosion Science and Technology
Beijing Institute of Technology, Beijing
100081, P. R. China
**e-mail: wuyqing@bit.edu.cn*
[b] *H. Guo*
Xi'an Modern Chemistry Research Institute
Xi'an, Shanxi Province, P. R. China

paratus could measure a fraction of the input energy and provide more quantifiable parameters for ignition at impact. In the present paper, we developed an image processing method of calculating the deformation, jetting, and flame expansion velocity, so that ignition and burning reaction violence of explosives could be quantitatively evaluated.

1.3 Hotspot-Ignition

It has long been recognized that some form of energy localization (hotspots) must occur under drop-weight impact, thereby first inducing localized chemical reaction, namely, ignition [26]. Walley et al. [3] conceived the highly fruitful idea of the localized hot spot and found that initiation mechanisms specific to explosive crystals are bound up with the anisotropy of plasticity and fracture in these crystals. Various sources of hotspots have been summarized by Field and Walley et al. [3, 27, 28], including collapse of gas spaces (producing shocks by jet impact or heating by adiabatic compression), localized adiabatic shear bands, friction, and viscous heating. Wu et al. [29] developed a thermal-mechanical model for the ignition of a layer of HMX particles under drop-weight impact. The model described heat deposition due to the contact deformation and friction, fracture of particles, melting, and chemical reaction at particle level simultaneously. Elban and Armstrong [30] showed that, in drop-weight impact tests, anisotropy in the crystal structure of RDX contributed to localization of shear failure in regions that had been indented during Knoop micro-hardness testing. Although many scholars have investigated possible hotspot mechanisms for explosives [31–35], the dominant mechanism for granular explosives under drop-impact still to be determined [36].

1.4 Combustion

In general, hotspots may survive and grow in size due to interaction or quench due to heat loss. If a hot spot with sufficient size is generated within an explosive material, the reaction may grow into a slow-burning region or a more explosion (initiation) [37]. In other words, once ignition occurs in an explosive, the question then becomes what the resulting violence will be. Therefore, it is desirable to get insight into both the evolution process of hotspots and evaluate the development of combustion following ignition. However, to the authors' knowledge, there are limited experimental investigations focused on combustion features of granular explosives under drop-weight impact.

1.5 Current Work

In the present study, a drop-weight impact apparatus equipped with high-speed camera was employed to examine the hotspots evolution and combustion development following ignition of RDX/HMX explosive. The jetting and burning phenomena of RDX and HMX were analyzed based on a large number of experimental observations. Furthermore, two types of paper, namely, waxed (high-roughness) and tissue (water-absorbing quality) paper, were put on the glass anvil for examining the heat-generation mechanisms of ignition and burning. An image processing method was developed to provide specific and quantitative indicators of different stages of mechanical and reaction response in drop-weight experiments. The ultimate goal of the present study is to understand how ignition and burning relate to the mechanical and physical processes, such as deformation, melting, and fragmentation, and improve our understanding level for accidental initiations of high explosives.

2 Experimental Configuration

2.1 Modified Drop-Weight Apparatus

The falling components and bottom base anvil ($\Phi 70 \times 100$ mm) of the drop-weight machine were modified, allowing high-speed photographic observations on dynamic responses of explosive particles. Both the striker and anvil were made from cast iron, in which grooves were machined to place mirrors and toughened glasses ($\Phi 50 \times 20$ mm), as shown in Figure 1. The dropped hammer with 5.782 kg can move along the vertical guide tracks. The schematic of the global light path in dotted line is shown in Figure 2. The target material is placed between two toughened glass anvils. The height of an LED electric light source was adjusted prior to impact, to be aligned with the upper embedded mirror. The photographs were taken at 6.67 μs frame interval using a low-light-level FASTCAM SA5 LOOOK C3 high-speed camera produced by Photron Corporation. An extra micro-lens is attached to the original lens for taking amplified photos of the millimeter-scale particles.

To test the practicability of the drop-weight device, impact experiments on a single sugar particle was first performed. In the absence of chemical reaction, Figure 3 shows that the apparatus is capable of observing inert materials. Initial brightness observed previously disappeared at 140 μs, which appears to be the result of crushing. The crushing stage extended to a maximum range of 714 μs. A larger range of blackness in the middle of the sample implies a large amount of crushed substance. For inert sugar, the area expansion motion was not so severe.

Figure 1. Photographs of (a) modified falling hammer (b) anvil base and (c) toughened glass.

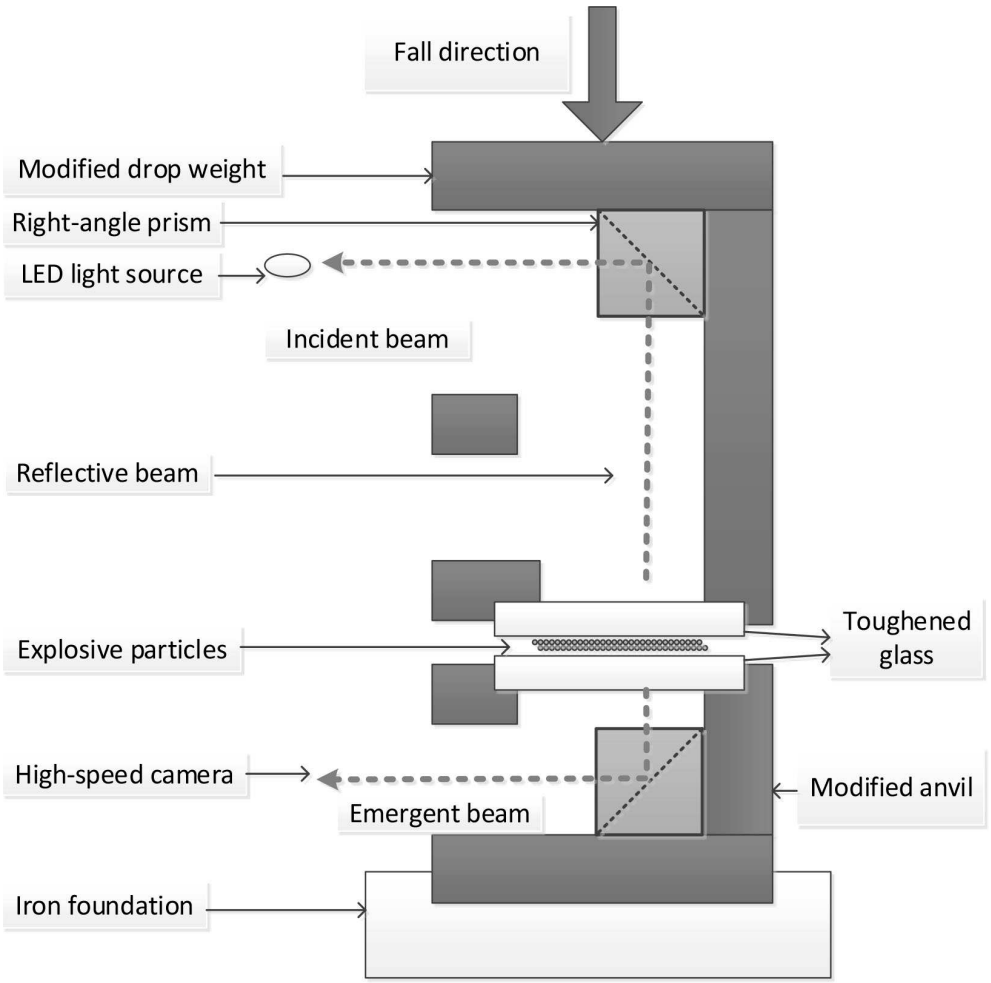

Figure 2. Schematic of the modified drop-weight machine equipped with optical system.

2.2 Micro-Morphology of Granular RDX/HMX

Two kinds of secondary high explosives, RDX and HMX, were used in our experiments. To exclude many complex factors inside a layer of explosive particles, a single explosive particle was selected as an appropriate object for the present research. Figures 4(a–f) show the micro-morphology of RDX and HMX particles taken by scanning electron microscope (SEM) and optical microscope (OM). Ellipsoidal RDX samples had an average particle size of around 50 ~ 60 μm and relatively smooth surfaces without evident sharp corners. Tiny pits and pores can be observed on RDX

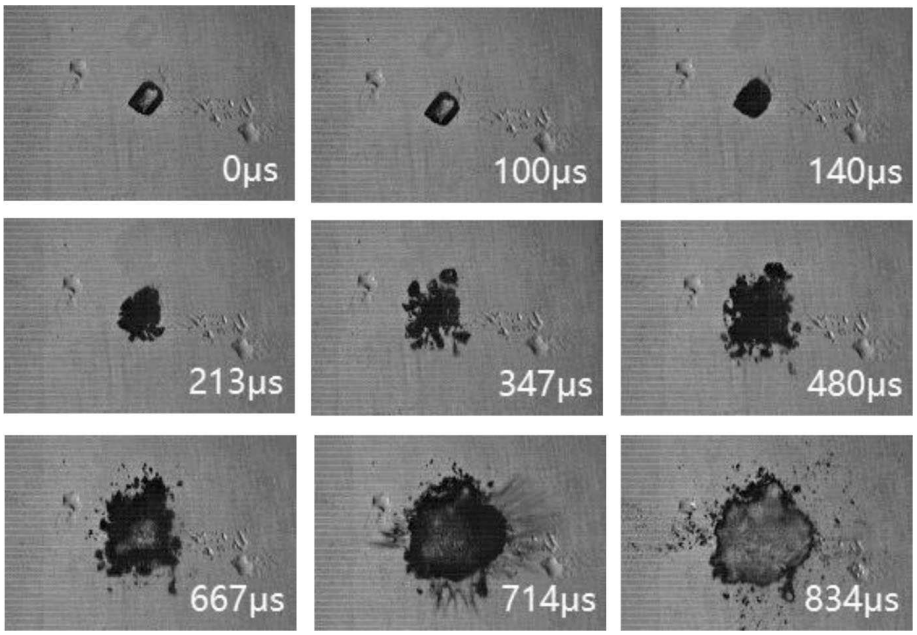

Figure 3. High speed photographic frames for impacted an individual sugar particle.

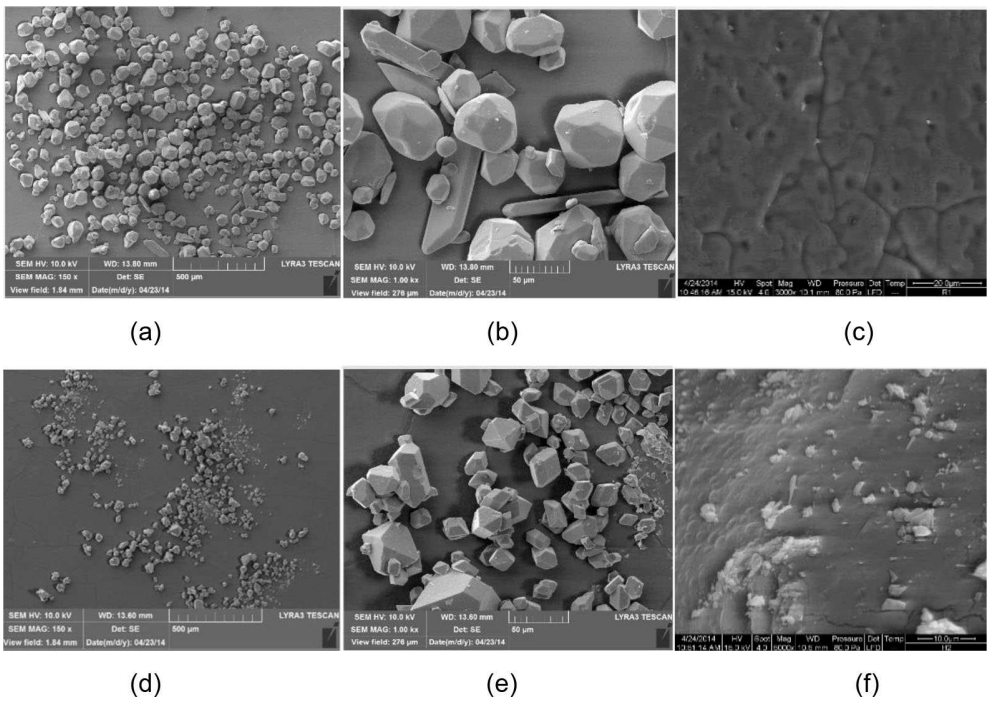

Figure 4. Micro-morphology of (a-c) RDX particles and (d-f) HMX particles employed in experiments observed using Scanning Electron Microscopy (SEM) [(a)(b)(d)(e)] and Optical Microscopy (OM) [(c)(f)].

particle surfaces. HMX consisted of more irregularly shaped powdery and granular forms. The size is in the range of 20–50 μm. More edges and corners and lots of small fragments in HMX powder surface can be observed. Hot-spots ignition induced by rapid air compression probably emerge in these defects during shock initiation.

3 Results for Granular Explosives

3.1 Jetting Phenomena

To identify the specificity of reactive materials due to ignition and burning process, responses of one RDX and salt particles were compared under simultaneous impact loading. Figures 5 and 6 showcases of no ignition for RDX together with salt particles under 10 and 15 cm drop-height impact respectively. The frequency of the HSC was chosen to be 150000 frames per second.

Figure 5 shows that the whole experiment process lasted approximately 1093 μs, both the RDX and salt particles fractured and compacted in a very similar way. Once those fragments were crushed into smaller pieces, a bright area appears in the middle of the RDX sample at 340 μs, which was earlier than that in salt (at 580 μs). Subsequently, the volume of the transparent region continued to increase until 580 μs and the jetting phenomenon was observed at 587 and 594 μs for the RDX sample. Both particles experienced deformation, breakage, partial melting (with color turning to milky), area expansion, and compaction during the whole process. The most noteworthy difference between the RDX and salt particles is that the former suddenly jetted following the appearance of brightness. RDX fragments in images at 587 and 594 μs showed behavior similar to splashing resulting in sudden expansion of covering area at the instant of jetting.

Figure 6 shows that jetting in RDX occurs at various sites and different moments from 620 to 747 μs. For RDX, jetting mostly follows full breakage and the appearance of milky color. Figures 5 and 6 show that even if there is no macroscopical combustion for reactive material, it still can exhibit significant difference to inert material due to its localized reaction. Jetting is just caused by localized chemical reaction. This may be an adequate method for understanding the hazard characterization of explosives. The idea that jetting corresponds to hot-spots ignition in crushed RDX and HMX samples is reasonable. From images by time sequences, time-to-ignition which is regarded as an important indicator of sensitivity can easily be determined.

To deeply understand all the stages that single energetic particle undergoes, selected frames for impacted RDX particle subjected to 5, 10, 15, and 20 cm drop-height impacts were presented in Figures 7–10 respectively.

In Figure 7, the process from 0 to 433 μs can be regarded as the pure mechanical stages in terms of area extension movement. From 500 μs, bright area appears and extends towards the boundary. Once ignition occurs, gas production will push surrounding powdery or liquid substances. Splashing due to fast motion of solid and/or liquid phase takes place, as shown from images from 660 to 700 μs. Non-uniform radial splashing reflects the inhomogeneous distribution of broken fragments, as well as violence of localized ignition reaction. With the sample cooling and pressure decreasing, violence of jetting gradually became weaker and weaker till 747 μs. In the final stage, no visible burning front appeared so that this particular impact test left a substantial amount of unreacted explosives. This case is a typical case that only ignition but no growth to burning happened.

All the graphs in Figures 8, 9, and 10 show that jetting phenomena are so common for reactive RDX explosives. Igni-

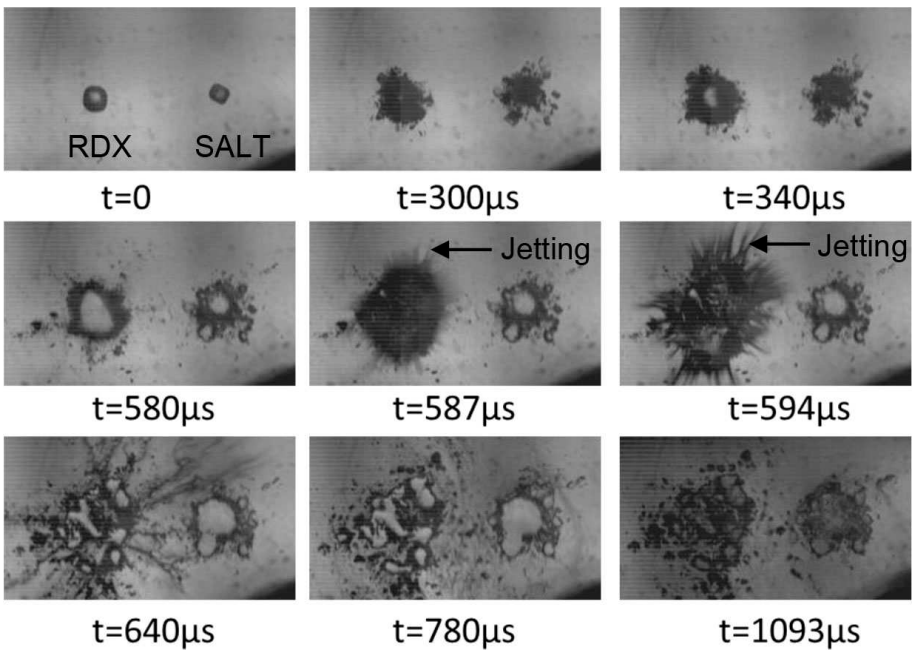

Figure 5. Comparison of one single RDX (left) and salt particle (right) under simultaneous 10 cm drop height impact.

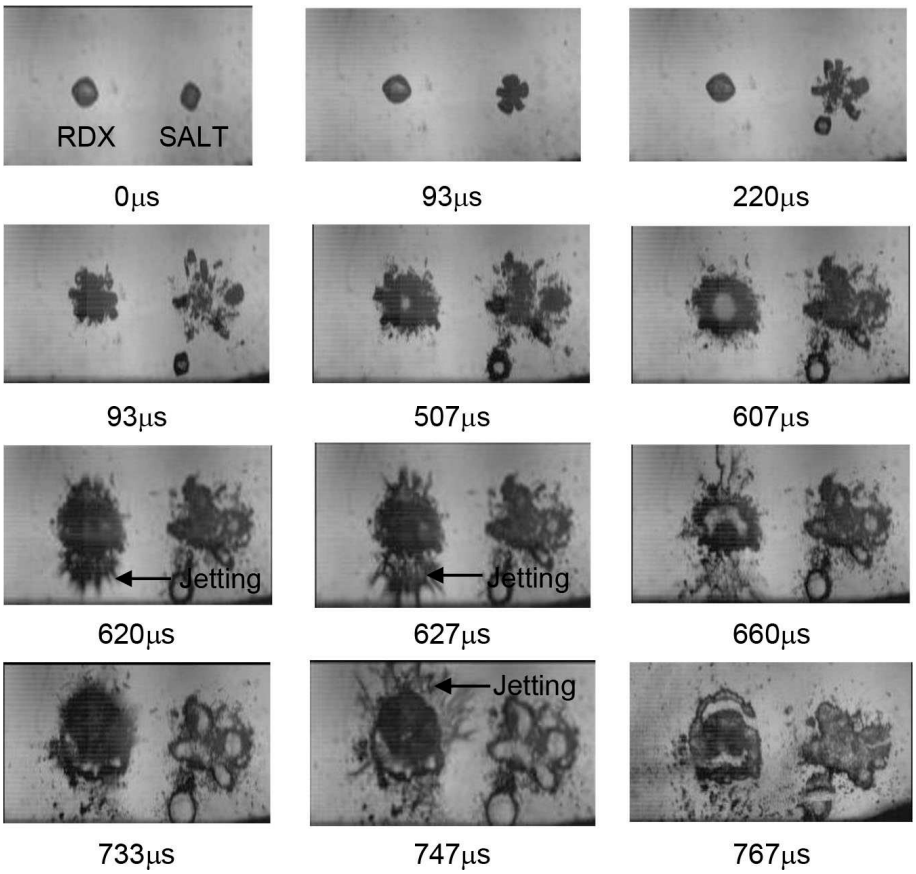

Figure 6. Comparison of one single RDX (left) and salt particle (right) under simultaneous 15 cm drop height impact.

tion starting times are determined to be 400, 366, and 280 μs respectively according to jetting occurrence in sequential images. These results also reflect the rule that ignition time under impact decreases with the increase of drop height. Milky color should be the combination effects of solid phase transition and local melting accompanied by ignition. Following ignition, a wide range of non-uniform chemical reaction usually occurs across the whole sample. As shown in Figure 8 (440 μs), Figure 9 (420 and 426 μs), and Figure 10 (306 and 353 μs), chemical reaction developed from the early to the end of ignition stage. Jetting phenomena can reflect the violence of ignition process (from weak to strong). Scattered radial traces result from anisotropic solids fragments motion driven by orientation-dependent gas production during ignition growth to deflagration.

Interestingly, a common feature exists in Figures 7–10, namely, burning fronts have not grown up macroscopically. Cooled solid fragments tend to become grey-colored area in which relatively narrow bands easily formed before the end of impact. Deflagration of impacted RDX single particle could not occur easily. From Figures 7–10, milky color at the central of RDX sample seems to imply the change of state. A large number of experiments of impacted RDX particle placed on toughened glass showed that only breakage, color change, compaction, and splashing but no burning or deflagration occurred below 10 cm drop-height.

For HMX particles, some of the phenomena are similar to RDX. Figure 11 compares one single HMX with a salt particle under 10 cm drop-height impact. Both materials underwent similar breakage and area expansion stages to a certain level. The salt particle showed obvious melting with a bright area in the middle of the sample at 407 μs, but no melting features in the HMX domain were observed until the end of the impact process. There was a small splash on the lower-left corner in HMX sample at 407 μs, while strong jetting occurred across almost the whole HMX particle at two sequential moments, 553 and 560 μs.

In Figure 12, there was a small splash on the upper right corner at 313 μs, while strong jetting occurred in almost the whole HMX sample at two sequential moments, 627 and 634 μs. A bright flame at 627 μs reflects development of combustion flame from ignited hot-spots. The flame soon extinguished without extending towards the bulk HMX sample. Compared with RDX, the difference is that jetting and flame in HMX developed from its solid phase. For the salt particle, only breakage, compaction, melting, and cooling took place in sequence but no jetting occurs.

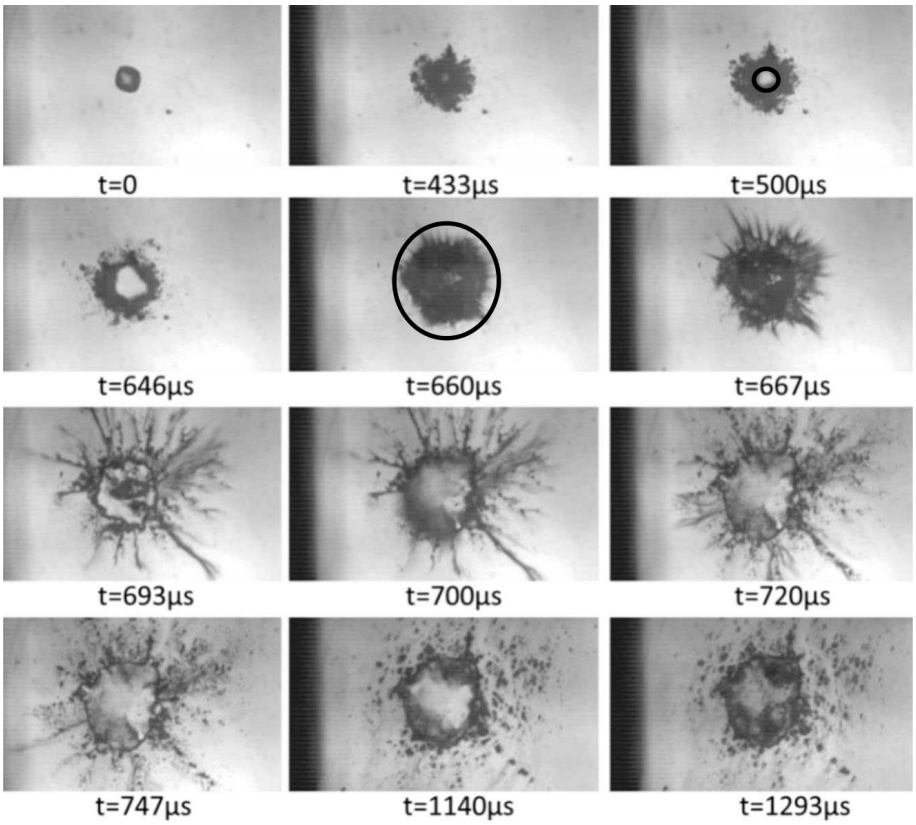

Figure 7. Selected high-speed photographic frames of one single RDX particle under 5 cm drop height impact.

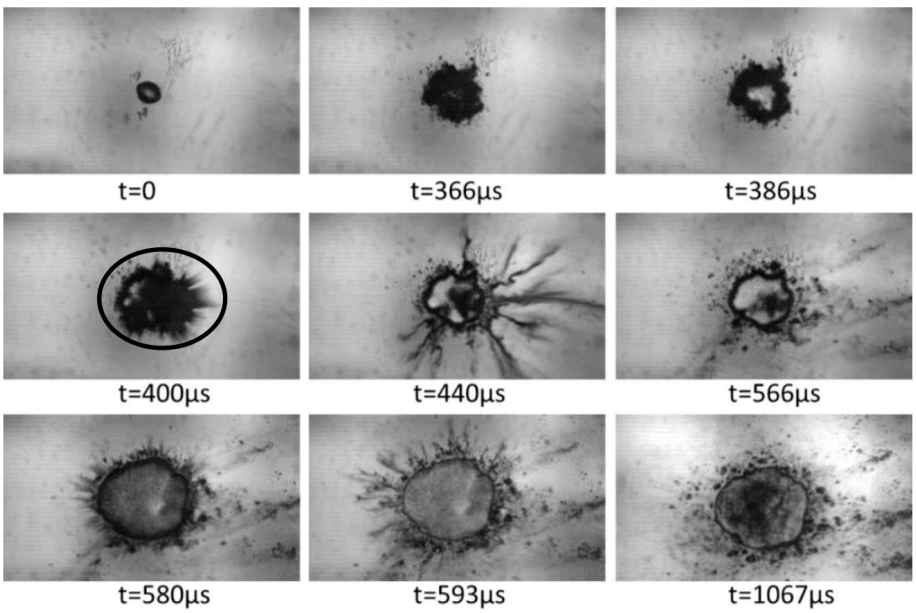

Figure 8. Selected high-speed photographic frames of one single RDX particle under 10 cm drop height impact.

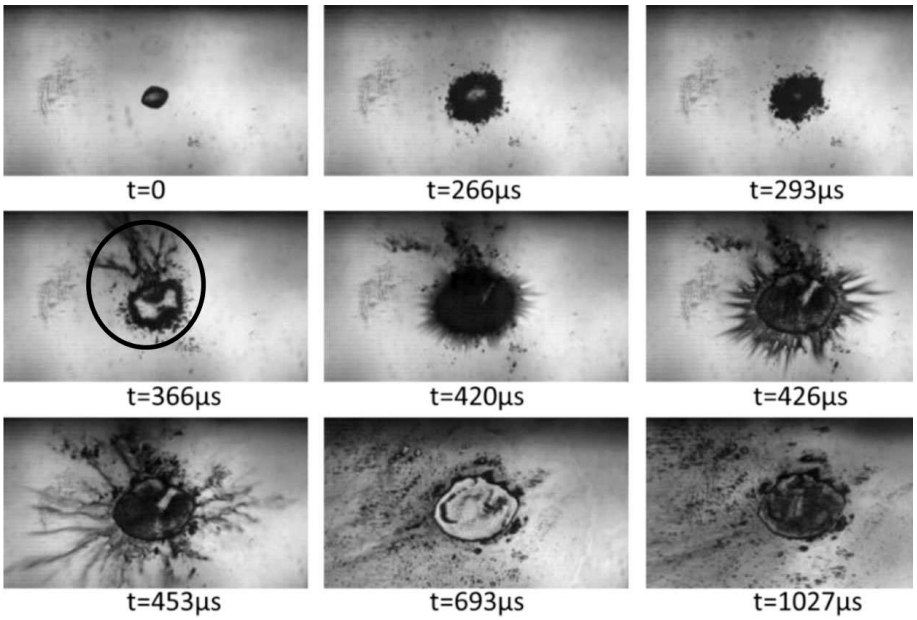

Figure 9. Selected high-speed photographic frames of one single RDX particle under 15 cm drop height impact.

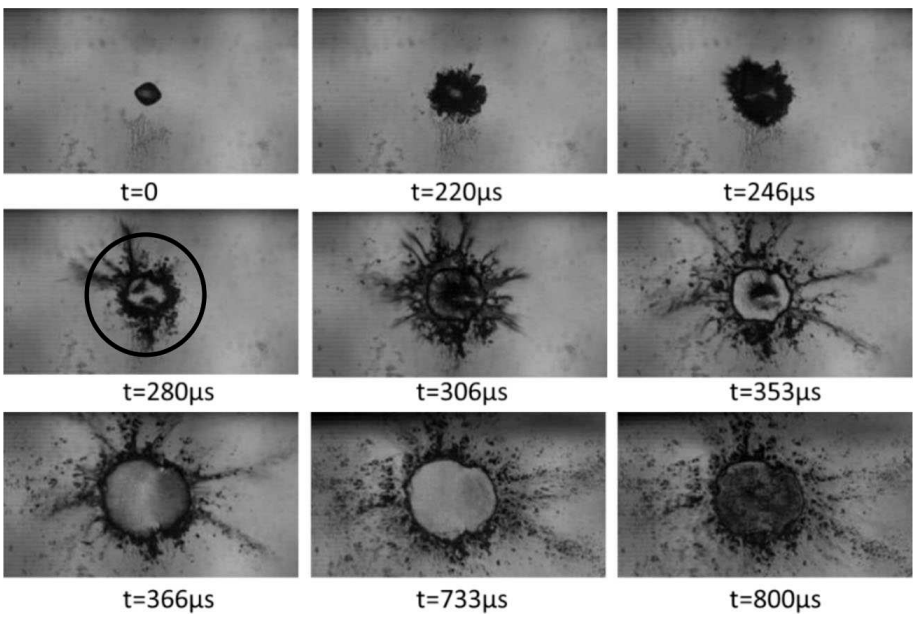

Figure 10. Selected high-speed photographic frames of one single RDX particle under 20 cm drop height

3.2 Burning of Single HMX/RDX Particle

In the above section, only breakage, compaction, small scale of area expansion, and strong jetting occur. No burning was observed during the whole experimental process. Figure 13 shows that intense jetting and burning took place almost at the same time for the HMX particle under 5 cm impact (i.e. 1634 μs). The flame extinguished quickly at the next moment (i.e. 1640 μs).

With the drop height increased to 10 cm, strong jetting at a very small fraction occurred at 440 μs, as shown in Figure 14. At 540 μs, burning flame suddenly developed and then suddenly extinguished at 546 μs. Only a small range of intense jetting occurs in Figures 13 and 14 during the whole process unlike RDX in Figures 7–10. When the drop height was increased to 15 cm, as shown in Figure 15, intense jetting can be observed around the HMX sample's

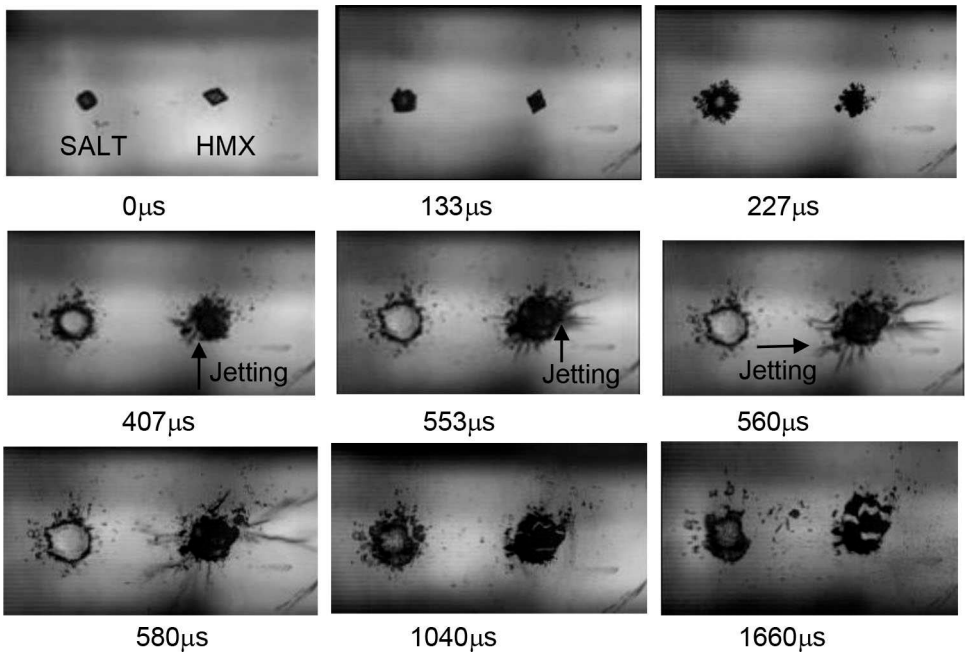

Figure 11. Comparison of one HMX (right) and one salt particle (left) under 10 cm drop-height impact simultaneously.

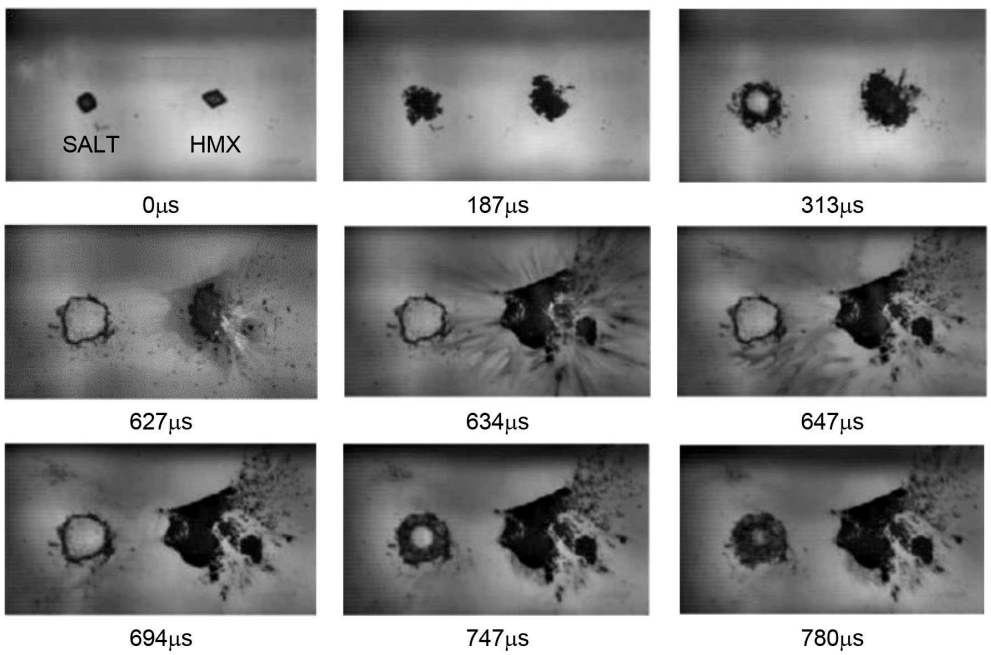

Figure 12. Comparison of one single HMX (right) and salt particle (left) under 15 cm drop height impact simultaneously.

boundary from 306 to 366 μs. We can discern that jetting phenomena last for a longer time with higher drop heights.

The previous experimental results showed that the probability of burning for an RDX particle is lower than that of HMX particle under the same impact loading. For drop-heights less than 15 cm, no burning flame was observed for an RDX single particle. Combustion in impacted RDX explosive particles was observed till the hammer height was increased to 15 cm. One burning case from five experiments of RDX single particle under 15 cm drop-height. However, we found that three burning cases from five experiments of RDX single particles under 20 cm drop-height (as shown in Figure 16). Local jetting occurs at the upper right corner at 260 μs in the broken sample. After large-scale jetting along with the whole sample becom-

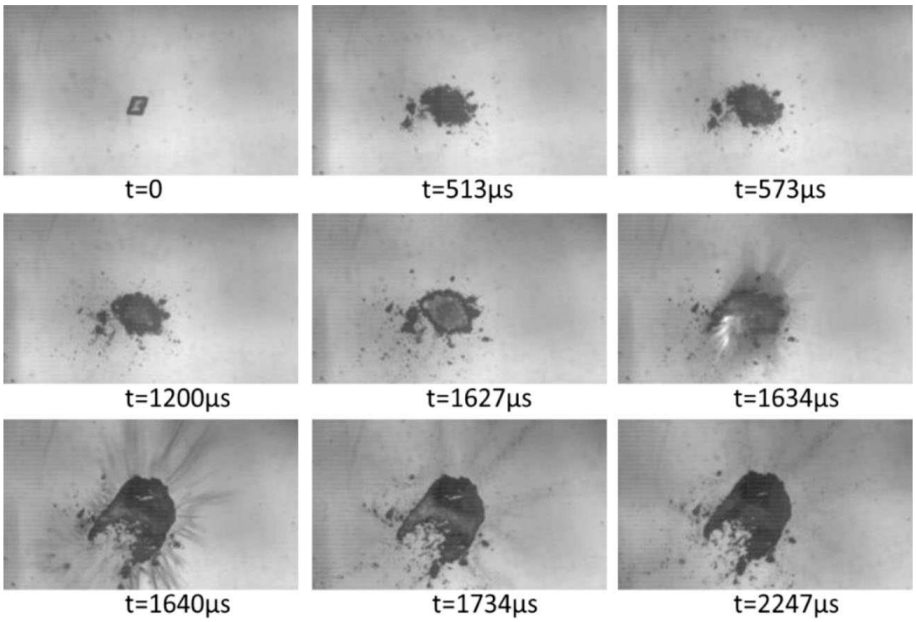

Figure 13. Selected high-speed photographic frames of an individual HMX particle under 5 cm drop height impact.

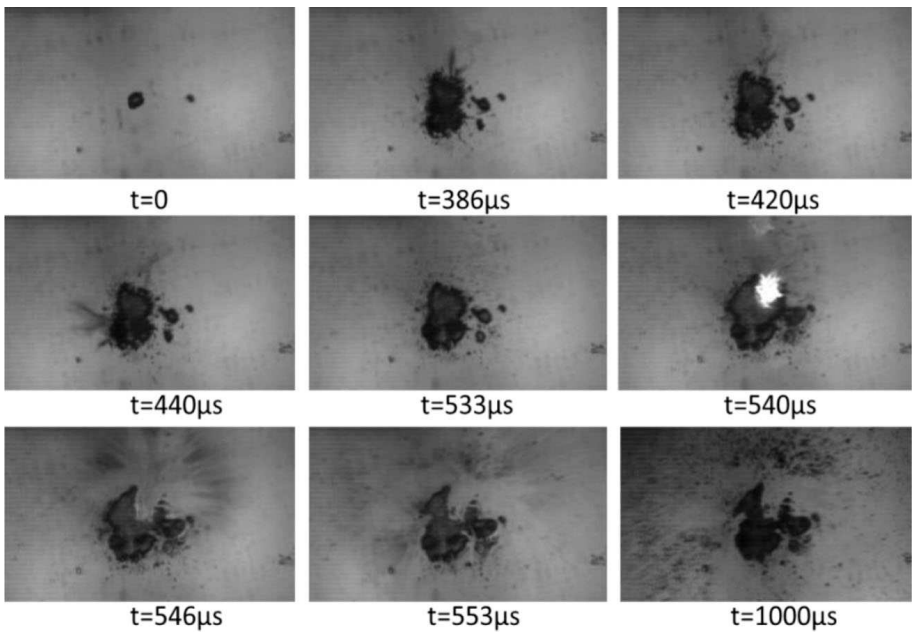

Figure 14. Selected high-speed photographic frames of an individual HMX particle under 10 cm drop height impact.

ing gray at 594 μs, local ignition region (marked by black line) leads to a small range of combustion seen from the graph of 600 and 607 μs.

3.3 Characterization of Impacted Responses

To quantitatively analyze the ignition-burning responses of RDX and HMX particles under drop-weight loading, several parameters such as radial deformation velocity (v_R), jetting velocity (v_J), and flame expansion velocity (v_F) were introduced. At first, the proportional relationship between the actual unit area and the number of pixels in high-speed images is required to be determined. A transparent ruler was placed on the toughened glass anvil before the start of experiments; then the image of the ruler was imported into Ps software, as shown in Figure 17. Two regions of length were drawn in the direction of the ruler, and they are of

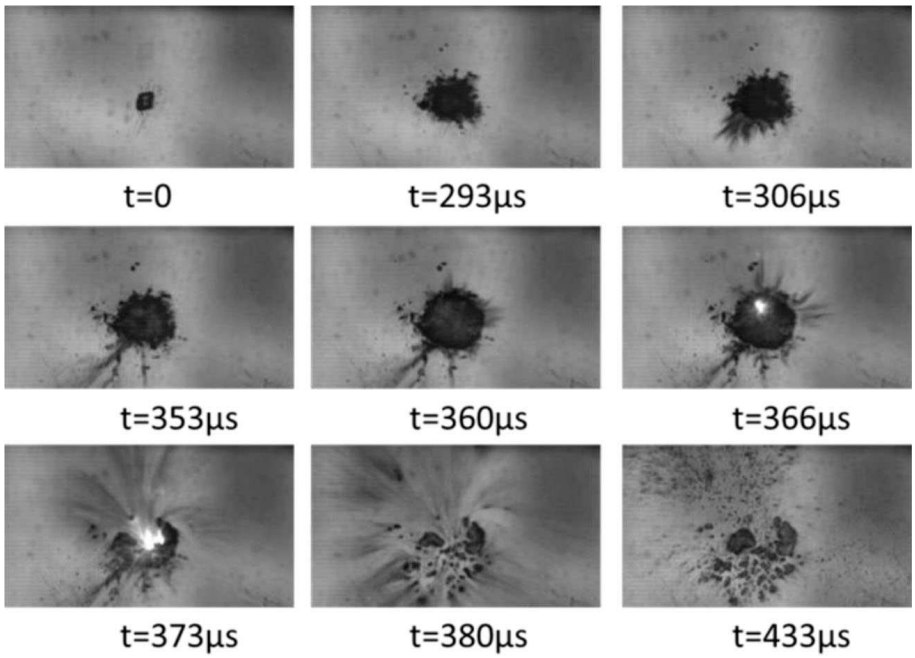

Figure 15. Selected high-speed photographic frames of an individual HMX particle under 15 cm drop height impact.

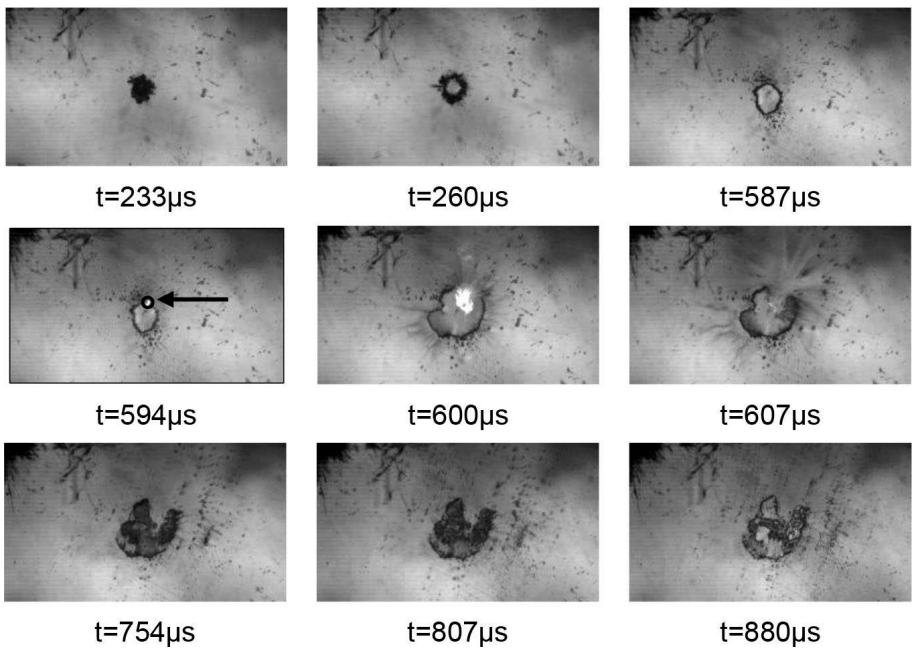

Figure 16. Selected high-speed photographic frames of an individual RDX particle under 20 cm drop height impact.

equal area with 8 square, millimeters on the rulers (The width is 4 mm and the height is 2 mm). The average number of pixels in the 8 square millimeters range (1674, 1612, 1638) is 1641.33. At the same time, we can know the mean pixel (27, 26, 26 pixels) of two millimeters is 26.33. This suggests that 26.33 pixels in the image represents 2 mm actually, namely, the dimensional scale $\beta = 26.33$ p/2 mm = 13.165 p/mm.

As mentioned in Section 3.1, jetting can usually be observed in the drop-weight impact experiments of RDX and HMX particles whether burning happened or not. In this section, jetting velocity is introduced to quantify the violence of local chemical reactions. Taking selected frames of

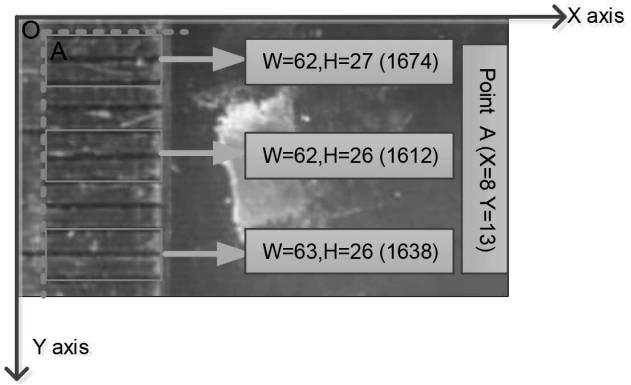

Figure 17. Calibration of proportional relation between actual unit area and the number of pixels in high-speed images. (The red dotted line is the coordinate line of second reference).

a single RDX particle under 10 cm drop-height impact (Figure 18) as an example, original jetting arose at 347 μs on the upper right edge and intense jetting was observed at 474 μs. To distinguish deformation and jetting events, the radial deformation velocity (v_R) is first calculated to characterize the stage of deformation. In Figures 18(a–b), the radial deformation velocity of an individual RDX particle after impact can be derived from frames of 0 and 313 μs with the dimensional scale $\beta = 13.165$ p/mm. From the area of value of P_1 ($P_1 = 132$) and P_2 ($P_2 = 1208$), we can know that two radius (R_1 and R_2).

The radial deformation velocity is given by:

$$P_1 = \pi R_1^2 \rightarrow R_1 = \sqrt{P_1/\pi} = \sqrt{132/\pi} = 6.48$$

$$P_2 = \pi R_2^2 \rightarrow R_2 = \sqrt{P_2/\pi} = \sqrt{1208/\pi} = 19.61$$

$$v_R = \frac{R_2 - R_1/\beta}{t} = \frac{\left(19.61 - 6.48/13.165\right)\text{mm}}{313\mu\text{s}} = 3.2\ \text{m/s}$$

The jetting velocity along three different directions are:

$$v_{J1} = \frac{P_{L1}/\beta}{t} = \frac{\left(32/13.165\right)\text{mm}}{(394-347)\mu\text{s}} = 51.72\ \text{m/s};$$

$$v_{J2} = \frac{P_{L2}/\beta}{t} = \frac{\left(50/13.165\right)\text{mm}}{(520-474)\mu\text{s}} = 82.56\ \text{m/s};$$

$$v_{J3} = \frac{P_{L3}/\beta}{t} = \frac{\left(44/13.165\right)\text{mm}}{(520-474)\mu\text{s}} = 72.66\ \text{m/s}.$$

According to the calculated results, the radial deformation velocity of RDX particle is much smaller than its jetting velocity ($v_R < v_J$), indicating that jetting events are barely affected by the solid deformation stage. Under the same drop-height impact, the radial deformation velocity of an HMX particle has approximated the same value of RDX (3.2 m/s). In contrast, the maximal jetting velocity of HMX is higher than the value of RDX. These two results indicate that HMX particles undergo a more violent chemical reaction than RDX, and the mechanical properties of two types of energetic particles (HMX & RDX) are relatively similar.

Once combustion occurs, the area expansion increases abruptly and the increment of area expansion can be employed to calculate the flame expansion velocity (v_F). As for the combustion of a single RDX particle under 20 cm drop-

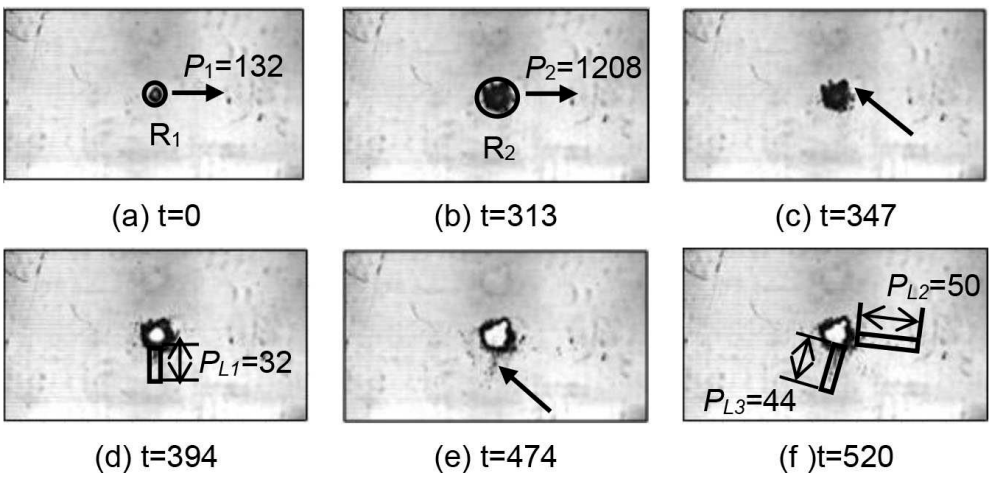

Figure 18. Measurement of the radial deformation velocity and jetting velocity of an individual RDX particle under 10 cm drop-height impact. (R_1 and R_2 represent the radii of P_1 and P_2)

height [Figure 19(a), two selected frames from Figure 16], the broken and melted RDX ignited at 594 μs and began to burn at 600 μs. The resolution ratio of the image in Figure 19 is 256×144 with total pixel (P_0 = 36864) and total area (S_0 = 122.58 mm^2). At the same moment, the combustion area (S_A) was proportional to the pixel quantity in the selected combustion region (P_A) by $S_A/S_0 = P_A/P_0$. The shape of the occupied combustion area is generally irregular and can be equivalent to a circle, thereby calculating the radius of equivalent circle (R) by $R = (S_A/\pi)^{1/2}$. The flame propagation velocity (v_F) equals the ratio of the difference between R_i and R_{i-1} during the selected time interval Δt.

The calculated value of v_F for a single RDX particle in terms of Figure 19(a) is 59.97 m/s. In contrast, the calculated value of v_F of a single HMX particle under 20 cm drop-height [Figure 19(b)] is lower than the value of RDX. This phenomenon is because that RDX sample was ignited after partial melting and formation of liquid phase; in contrast, there is no obvious melting observed for HMX sample before ignition. Thus, the flame propagation velocity in the liquid phase (RDX) is higher than the propagation velocity in the broken-solid phase (HMX).

Taking selected three frames of a single HMX particle under 10 cm drop-height impact (Figure 20) as an example, original melting arose at 227 μs in the center and the maximum melting was observed at 580 μs. During the process, the small heated contact zones were assumed to be independent, resulting in a simple thermal condition around the heated contact regions. Although failure of the material leads to internal surfaces rubbing against each other and generating heat, most of the heat will be dispersed by fragments. Temperature rise due to contact deformation, frictional heating [38] and heat of chemical reaction can be obtained by

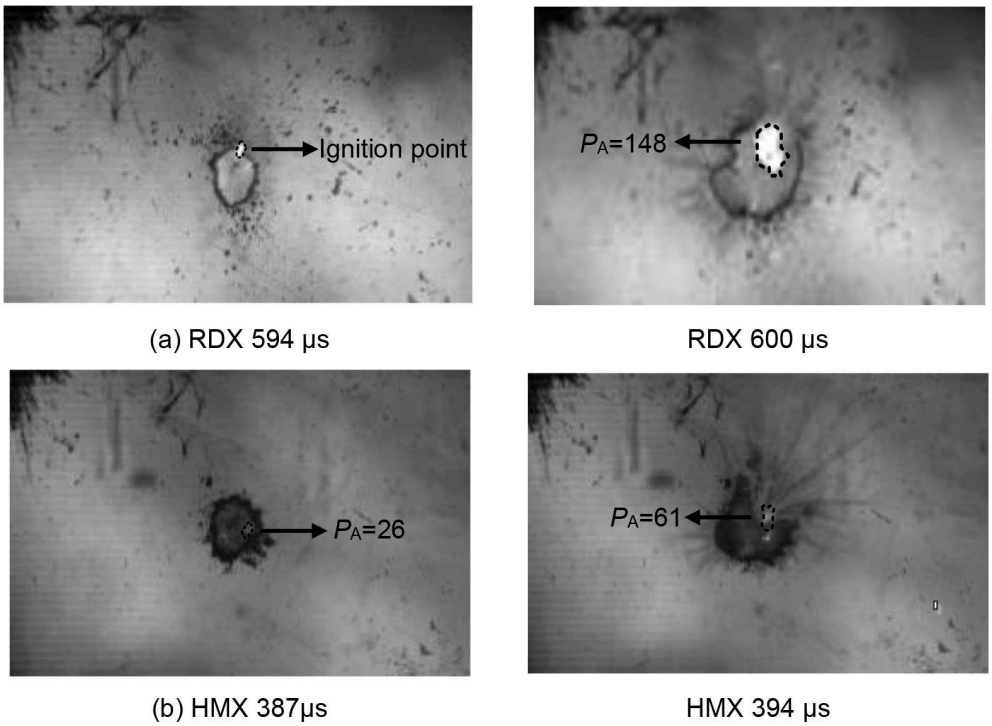

Figure 19. Selected high-speed photographic frames of one single (a) RDX and (b) HMX particle under 20 cm drop-height.

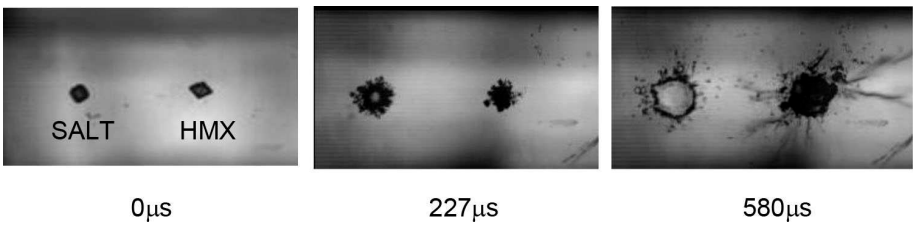

Figure 20. Proving the crystal melting of an individual HMX particle (right) under 10 cm drop-height impact.

$$\Delta T(t) = \underbrace{\frac{1}{2\rho_s c_s\sqrt{\pi k}}\int_0^{t_{load}}\frac{p_c(t)\dot{\delta}(t)}{(t_{load}-t)^{1/2}}\left\{1-exp\left[-\frac{\alpha^2(t)}{4k(t_{load}-t)}\right]\right\}dt}_{contact\,deformation\,dissipation} + \underbrace{\int_0^{t_{load}}\frac{\mu_f p_c(t)v_p(t)}{2\sqrt{\pi kt}}dt}_{friction\,heating} + \underbrace{\int_0^{t_{load}}\frac{1}{c}q_r Z_r exp(-E_A/R_gT)dt}_{chemical\,reaction\,heating}$$

where c_s is the specific heat, and k is the thermal diffusivity constant of the explosive material, $\delta(t)$ is the net impression depth of one particle in contact with the impacting surfaces, t_{load} is the loading time, ρ_s, $p_c(t)$, $v_p(t)$, $\alpha(t)$ and μ_f are the crystal density, an individual particle's pressure, radial expansion velocity, the contact radius and the net impression depth, q_r and $Z_r exp(-E_A/R_gT)$ are the decomposition reaction heat per unit mass and the Arrhenius expression for the reaction rate [39].

We can know that the temperature rise must cause crystal melting according to reference [38] and [39].

3.4 Heat-Generation Mechanisms and Role of Waxed/Tissue Paper

To make further investigations on the heat-generation mechanisms of ignition and burning, a piece of waxed paper was put on the glass anvil. As waxed paper has a certain light-transmission property, phenomena can still be observed using HSC. In Figure 21, one single RDX particle was impacted by a 10 cm drop-height. The particle experienced the sequence of fracture, breakage, compaction, gray color, jetting, ignition, and rapid combustion.

At 646 μs, when the gray color spreads to a large range, strong jetting appears at the next frame (at 653 μs). In this case, jetting is more likely to be limited in local regions compared with that on the glass anvil. Burning will be delayed and will not occur immediately after jetting. Till 713 μs, burning phenomenon developed in the upper region. The flame front continued to grow and propagated radially outwards till 727 μs. The waxed paper will be burned when the flame front develops. The flame tends to die out due to heat loss after the moment of 760 μs.

The recovered waxed paper with burned traces left due to reacted RDX particle are presented in Figure 22. The hotspots center and its development path from ignition to combustion can be seen on the waxed paper.

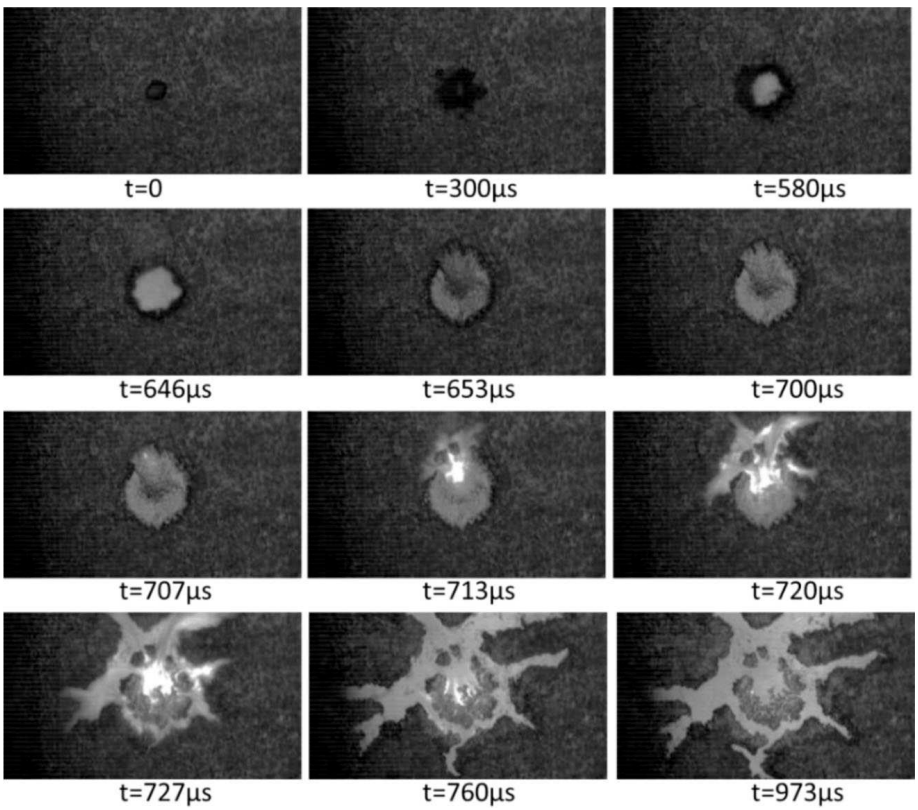

Figure 21. Selected high-speed photographic frames of an individual RDX particle on a kind of waxed paper under 10 cm drop height impact.

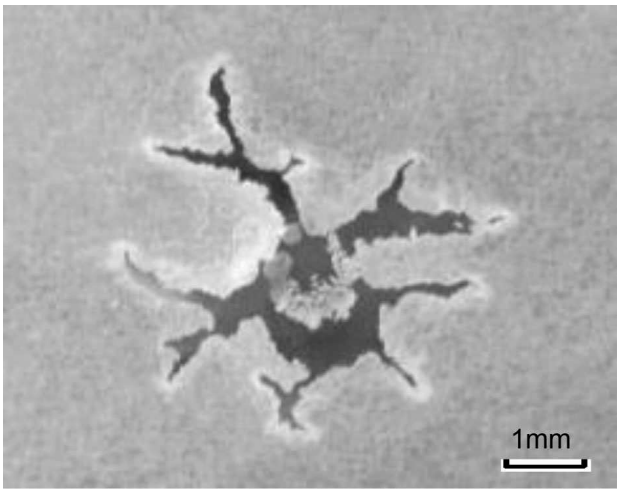

Figure 22. Recovered waxed paper below the RDX sample after impact.

Figure 23 provides another case of an RDX particle on waxed paper under 10 cm drop-height impact. Two burning sources were observed at 746.7 μs. The whole process of compaction, fragmentation, ignition, burn front development can be observed. Before burning occurs, grey-white color expands from a small spot (at 446.7 μs) to a large range (at 720 μs). The waxed paper has negative effects on powder splashing. Therefore, no obvious jetting appears for an RDX particle on the waxed paper as shown in Figure 23. Due to no excessive heat loss through jetting, hot spots are more likely to grow into burning cores.

For the sake of examining the underlying mechanisms of the ignition process, residues of impacted RDX particle samples on waxed paper were collected. Figure 24 show optical microscope images of the unreacted residues of RDX samples. It's interesting to notice that there are traces of crystallization in the comminuted RDX [Figure 24(a)]. In Figures 24(b–d), the magnified image marked by a black circle shows that molten substance has flowed into the waxed paper pores. This implied that solid-liquid phase change is common for impacted RDX.

Statistical analyses of ten impact experiments of RDX explosive single particles with waxed paper substrate gave 60% burning probability instead of 10% probability on glass anvil under 10 cm drop-height impact. We understand as glass surface is smooth that liquid phase substance

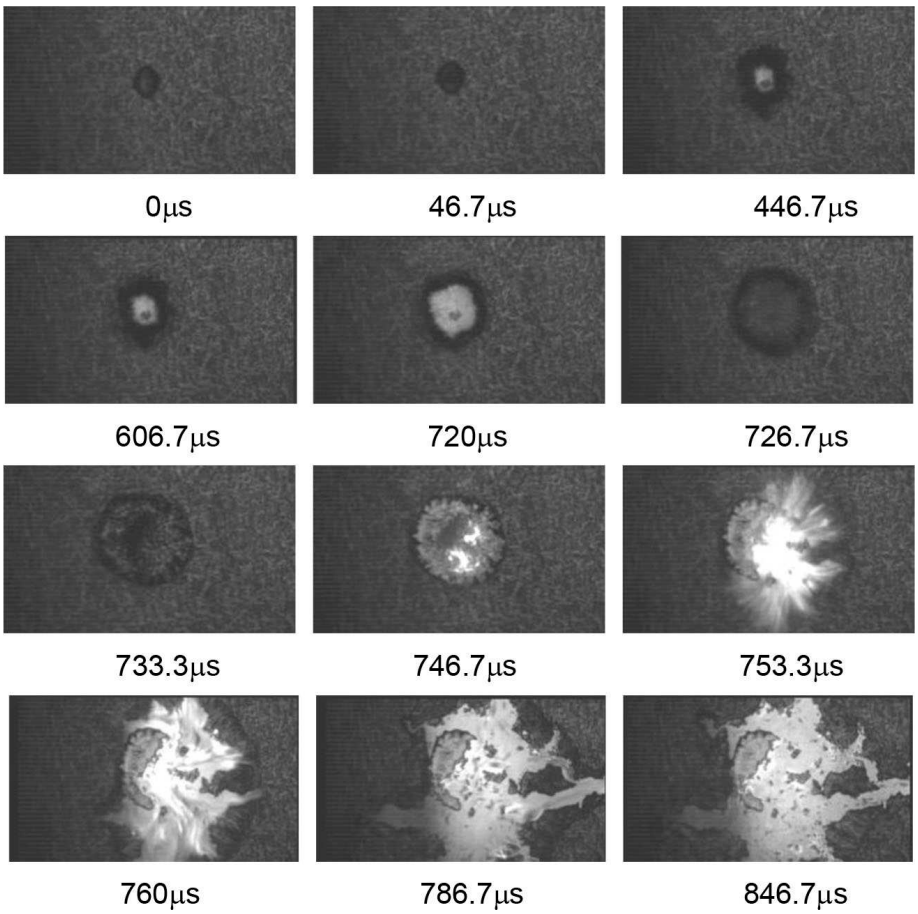

Figure 23. Another case of an individual RDX particle on waxed paper under 10 cm drop-weight impact.

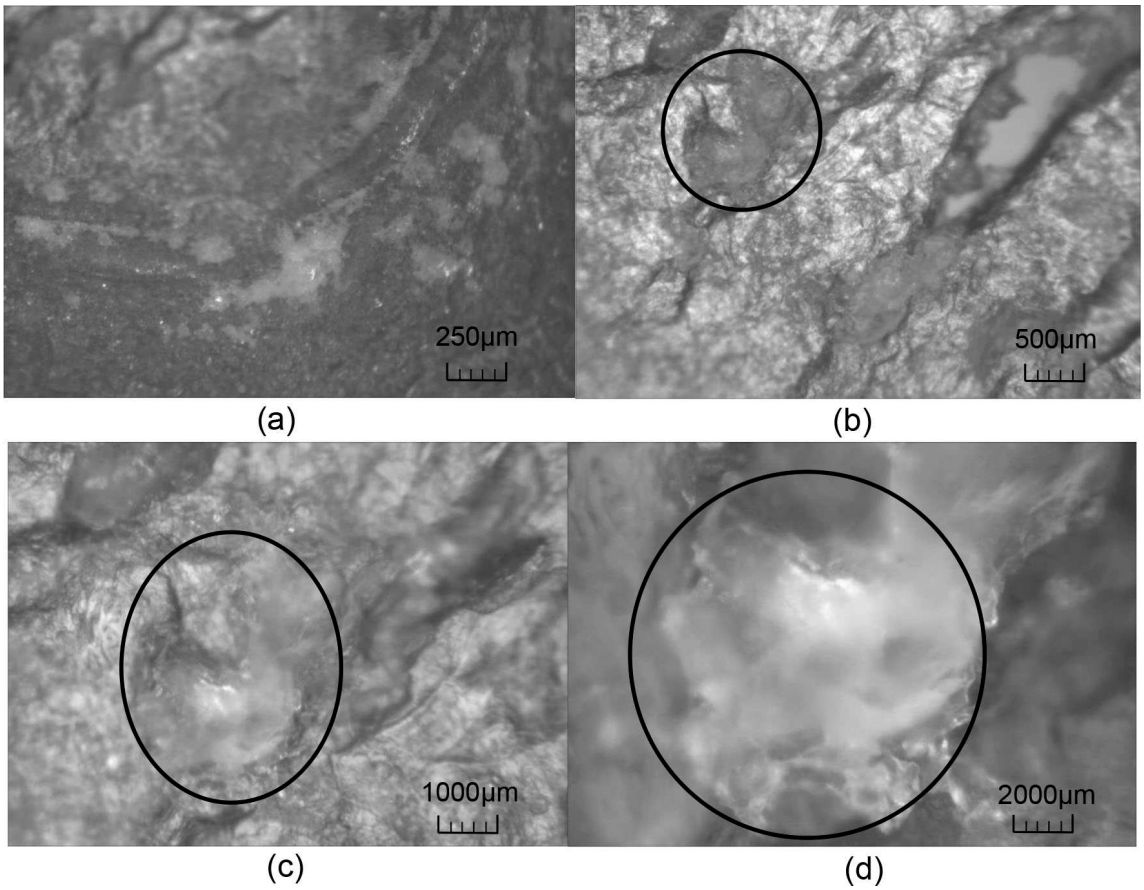

Figure 24. Optical microscope observations of the collected unreacted crushed RDX sample.

splashed out more easily. As localized energy releases through strong jetting, hot-spots growth process will be inhibited on glass anvil. When waxed paper was put beneath the RDX particle, non-uniform viscous flow along the pore channel. Small scale viscous flow heat-generation mechanism results in higher local temperature rise, thus increasing the possibility of ignition growth to burning.

However, tissue paper will reduce the impact sensitivity of RDX. The high-speed photography images for one RDX granule placed on tissue paper are presented in Figure 25. The light transmission of tissue paper is relatively poor so that the background is a little dark. No jetting and combustion and only gray-white color extension can be observed throughout the process. This can be explained by the fact that the liquid phase is easily absorbed by the tissue paper, thereby limiting the viscous flow. Viscous flow is the main heat generation mechanism in impacted RDX.

In addition, the high-speed photography images for one HMX granule placed on tissue paper are presented in Figure 26. According to the experiment, there seems to be an increase in ignition probability for impacted HMX on tissue paper. There was little liquid phase appearing for drop impacted HMX particle and we assume HMX ignites in solid phase. The main ignition mechanism should be frictional heat between fragments and base anvil, as well as between debris. As the tissue paper will increase the friction coefficient, relatively high-temperature rise due to friction heat is caused. Therefore, HMX ignition probability is greater than RDX on tissue paper. Further research on ignition mechanisms of the two explosives needs to be done in the future.

4 Discussions

The mechanical and physical mechanisms of ignition and burning growth should be studied to characterize the possible hazard of energetic crystals under drop-weight impact loading. In the present study, the experimental work gives particular emphasis on the mechanical-chemical responses using a drop-weight impact machine equipped with HSC. It has been found that jetting is the most obvious difference between reactive and inert particles. Jetting phenomenon is the result of the producing of gaseous products, which push the pulverized or melted explosives to splash radially. Thus, the time of appearance of jetting can be viewed as a sign of explosive ignition.

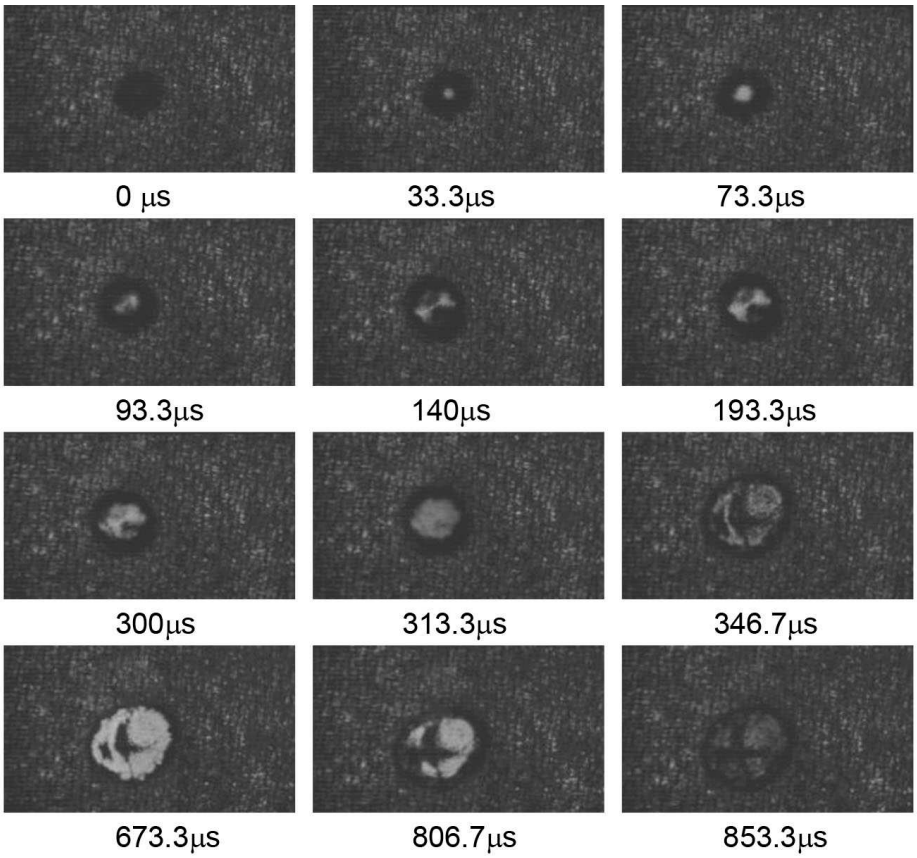

Figure 25. An individual RDX particle on tissue paper under 10 cm drop-weight impact.

The experimental results show that ignition of RDX generally takes place in the liquid phase after melting process, while ignition of HMX generally takes place in the solid phase after deformation and fragmentation process. Liquid RDX is easier to take sputter phenomenon than solid HMX, thereby producing additional heating due to viscous effects. Moreover, if a piece of tissue paper is put on the glass anvil, the impact sensitivity of RDX will be reduced. This can be explained by the fact that the liquid phase is easily absorbed by the tissue paper, thereby limiting heat generation by viscous flow. Therefore, we could infer that, under drop-weight impact, the dominant hotspots mechanism of RDX particles is heat generation due to viscous effects, and the hotspots mechanism of HMX particles is related to solid mechanics processes, such as localized plasticity, friction, or fracture.

Once the hotspots are formed, either they fail to react chemically because of thermal diffusion or they react exothermically creating an ignition site in the solid explosive. Therefore not only do we need to know when and where and how ignition occurs but also how violent the subsequent burning or explosion chemical reaction will be caused following ignition [36]. The combustion of the RDX sample can be transmitted to the whole sample, while the combustion of the HMX sample is most quickly extinguished. These phenomena indicate that combustion propagates more easily in the liquid-phase RDX sample than in the solid-phase HMX sample. Moreover, the results from image processing show that, given the same drop-height, the flame propagation velocity in the liquid phase (RDX) is higher than the propagation velocity in the broken-solid phase (HMX), indicating that reaction of RDX is more violent than the reaction of HMX.

To make further investigations on the heat-generation mechanisms of ignition and burning, a piece of waxed paper was put on the glass anvil. Due to the high-roughness quality of waxed paper, the jetting of liquid-phase RDX on the waxed paper is more likely to be limited to local regions compared with that on the glass anvil. The limitation of strong jetting for RDX on the waxed paper inhibits the release of localized energy, thereby contributing to the hotspots growth and burning process. This explanation can be verified by the statistical analyses of experimental observations, namely, the ignition growth to burning probability of RDX particle increases in the waxed paper case.

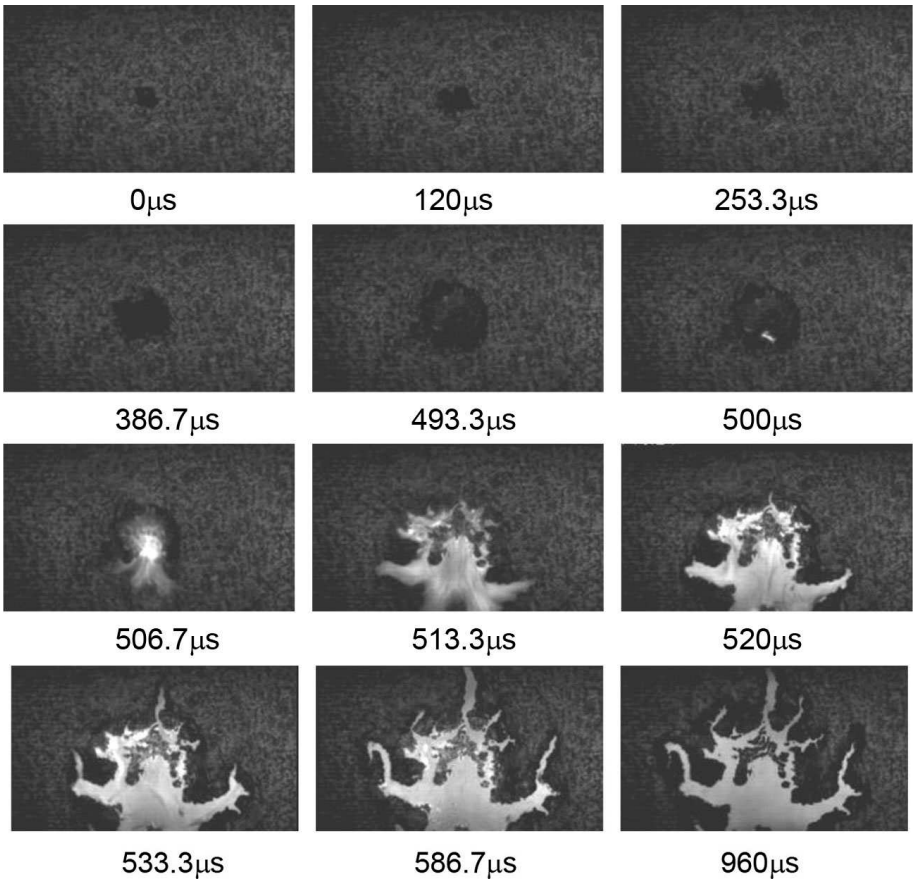

Figure 26. An individual HMX particle on tissue paper under 10 cm drop-weight impact.

5 Conclusions

The experimental analyses of hotspots evolution and combustion development of a series of RDX and HMX particles were performed based on the optimized drop-weight experimental system equipped with the HSC. Jetting phenomena is the result of the energy released by gaseous products, which can be used to mark the occurrence of ignition. For RDX sample, the molten phase plays an important role to the formation of the hot-spots. Hot-spots coalescence promotes flame propagation whose velocity reflects the violence of deflagration reaction. Deformation velocity, jetting velocity, and flame propagation velocity have been measured via an image processing method. The jetting of liquid-phase RDX on the waxed paper is limited to local regions compared with that on the glass anvil. In addition, burning probability of RDX particles increases for the waxed paper case.

In the future, both theoretical and numerical modeling for hotspot formation and growth to burning are desirable to deal with the complex thermal and chemical responses of explosive particles under drop-weight impact and provide instructive information for experiments.

Acknowledgements

The authors would like to thank the Science Challenging Program (TZ2016001) and China National Nature Science Foundation (Grant nos. 11572045 and 11872119) and Pre-research Project of Armament (No. 1421002020101-01) for supporting this project.

References

[1] C. W. An, F. S. Li, X. L. Song, Y. Wang, X. D. Guo, Surface coating of RDX with a composite of TNT and an energetic-polymer and its safety investigation, *Propellants Explos. Pyrotech.* **2009**, *34,* 400–405.

[2] K. Yang, Y. Q. Wu, F. L. Huang, Numerical simulations of microcrack-related damage and ignition behavior of mild-impacted polymer bonded explosives, *J. Hazard. Mater.* **2018**, *356,* 34–52.

[3] S. M. Walley, J. E. Field, M. W. Greenaway, Crystal sensitivities of energetic materials, *Mates. Sci. Technol.* **2006**, *22*, 402–413.

[4] S. Kim, Y. Wei, Y. Horie, M. Zhou, Prediction of shock initiation thresholds and ignition probability of polymer-bonded explosives using mesoscale simulations, *J. Mech. Phys. Solids.* **2018**, *114,* 97–116.

[5] A. Barua, Y. Horie, M. Zhou, Energy localization in HMX-Estane polymer-bonded explosives during impact loading, *J. Appl. Phys.* **2012**, *111,* 054902.

[6] L. M. Tavares, R. P. King, Single-particle fracture under impact loading. *Int. J. Miner. Process.* **1998**, *54*, 1–28.
[7] J. E. Balzer, J. E. Field, M. J. Gifford, W. G. Proud, S. M. Walley, High-speed photographic study of the drop-weight impact response of ultrafine and conventional PETN and RDX, *Combust. Flame*, **2002**, *130*, 298–306.
[8] J. E. Balzer, W. G. Proud, S. M. Walley, J. E. Field, High-speed photographic study of the drop-weight impact response of RDX/DOS mixtures, *Combust. Flame,* **2003**, *135,* 547–555.
[9] S. M. Walley, J. E.Field, S. J. P.Palmer, Impact Sensitivity of Propellants, *Proc. R. Soc. London* **1992**, *438*, 571–583.
[10] R W. Barley, Mineral comminution circuits: Their Operation and Optimisation, in: *Julius Kruttschnitt Mineral Research Centre,* Eds.: T. J. N. Munn, S. Morrell, R. D. Morrison, T. Kojovic, Queensland, Australia **1996**, 1–8.
[11] S. S. Narayanan, Single particle breakage tests: A review of principles and application to comminution modeling, *Bull. Proc. Australian. Inst. Min. Metall.* **1986**, *291,* 49–58.
[12] M. H. Keshavarz, Prediction of impact sensitivity of nitroaliphati, nitroaliphatic containging other functional groups and nitrate explosives, *J. Hazard. Mater.* **2007**, *148,* 648–652.
[13] R. W. Armstrong, C. S. Coffey, V. F. Devost, Crystal size dependence for impact initiation of cyclotrimethylenetrinitramine explosive, *J. Appl. Phys.* **1990**, *68,* 979–984.
[14] S. Zeman, New aspects of the impact reactivity of Nitramines, *Propellants Explos. Pyrotech.* **2000**, *25*, 66–74.
[15] B. M. Rice, J. J. Hare, A quantum mechanical investigation of the relation between impact sensitivity and the charge distribution in energetic molecules, *J. Phys. Chem. A.* **2002**, *106*, 1770–1783.
[16] M. H. Keshavarz, M. Jaafari, Investigation of the various structure parameters for predicting impact sensitivity of energetic molecules via artificial neural network, *Propellants Explos. Pyrotech.* **2006**, *31*, 216–225.
[17] M. H. Keshavarz, H. R. Pouretedal, A. Semnani, Novel correlation for predicting impact sensitivity of nitroheterocyclic energetic molecules, *J. Hazard. Mater.* **2007**, *141*, 803–807.
[18] M. H. Keshavarz, H. R. Pouretedal, Simple empirical method for prediction of impact sensitivity of selected class of explosives, *J. Hazard. Mater.* **2005**, *124*, 27–33.
[19] Y. Wen, X. Long, Y. Xiang, S. Yu, X. Dai, M. Li, Mass dependent of explosion probability of RDX, Tetryl, and a PBX powder in drop hammer test, *Propellants Explos. Pyrotech.* **2015**, *40*, 433–438.
[20] A. Mohamed, H. L. Michel, P. Christiaan, H. Michael, Statistical assessment methods for the sensitivity of energetic materials. *Propellants Explos. Pyrotech.* **2008**, *33*, 60–65.
[21] M. H. Keshavarz, Simple relationship for predicting impact sensitivity of Nitroaromatics, Nitramines, and Nirtoaliphatics. *Propellants Explos. Pyrotech.* **2010**, *35*, 175–181.
[22] J. G. Reynolds, P. C. Hsu, G. A. Hust, S. A. Strout, H. K. Springer, Hot spot formation in mock materials in impact sensitivity testing by drop hammer, *Propellants Explos. Pyrotech.* **2017**, *42*, 1303–1308.
[23] D. N. Preston, G. W. Brown, M. M. Sandstrom, C. J. Pollard, K. F. Warner, D. L. Remmers, J. G. Reynolds, Small-Scale safety testing of Ammonium Nitrate and mixtures, *Propellants Explos. Pyrotech.* **2016**, *41*, 9–13.
[24] L. M. Tavares, Energy absorbed in breakage of single particles in drop weight testing, *Miner. Eng.* **1999**, *12*, 43–50.
[25] V. S. Joshi, M. Elert, M. D. Furnish, R. Chau, N. Holmes, J. Nguyen, Recent developments in shear ignition of explosives using hybrid drop weight- Hopkinson bar apparatus, *AIP Conf. Proc.,* **2007**, *955*, 945–950.
[26] M. Akiki, S. Menon, A model for hot spot formation in shocked energetic materials, *Combust. Flame.* **2015**, *162*, 1759–1771.
[27] J. E. Field, G. M. Swallowe, S. N. Heavens, Ignition mechanisms of explosives during mechanical deformation, *Proc. R. Soc. London Ser. A* **1982**, *382*, 231–244.
[28] J. E. Field, Hot spot ignition mechanisms for explosives, *Acc. Chem. Res.* **1992**, *25*, 489–496.
[29] Y. Q. Wu, F. L. Huang, Ming Huang. Modeling of ignition in a single layer of impacted energetic crystals, *Propellants Explos. Pyrotech.* **2013**, *38*, 214–223.
[30] W. L. Elban, R. W. Armstrong, Microhardness study of RDX to assess localized deformation and its role in hot spot formation, in: *Proceedings of the 7th International Symposium on Detonation: June 16–19,* **1981**, 976–985.
[31] S. Ravindran, A. Tessema, A. Kidane, Multiscale damage evolution in polymer bonded sugar under dynamic loading, *Mech. Mater.* **2017**, *114*, 97–106.
[32] S. Kim, C. Miller, Y. Horie, C. Molek, E. Welle, M. Zhou, Computational prediction of probabilistic ignition threshold of pressed granular octahydro-1,3,5,7-tetranitro-1,2,3,5-tetrazocine (HMX) under shock loading, *J. Appl. Phys.* **2016**, *120*, 115902.
[33] R. Liu, P. W. Chen, Modeling ignition prediction of HMX-based polymer bonded explosives under low velocity impact, *Mech. Mater.* **2018**, *124*, 106–117.
[34] X. Song, X. Cheng, X. Yang, D. Li, R. Linghu, Correlation between the bond dissociation energies and impact sensitivities in nitramine and polynitro benzoate molecules with polynitro alkyl groupings, *J. Hazard. Mater.* **2008**, *150*, 317–321.
[35] D. Z. Guo, Q. An, W. A. Goddard, S. V. Zybin, F. Huang, Compressive shear reactive molecular dynamics studies indicating that cocrystals of TNT/CL-20 decrease sensitivity, *J. Phys. Chem. C.* **2014**, *118*, 30202–30208.
[36] K. Yang, Y. Q. Wu, F. L. Huang, M. Li, Numerical simulations of mechanical and ignition-deflagration responses for PBXs under low-to-medium-level velocity impact loading, *J. Hazard. Mater.* **2017**, *337*, 148–162.
[37] B. W. Asay, *Shock wave science and technology reference library* (Volume 5): *Non-Shock Initiation of Explosives*, Springer, Berlin, **2010**, 483–535.
[38] H. S. Carslaw, J. C. Jaeger, *Conduction of Heat in Solids*, Clarendon Press, Oxford, **1959**, pp. 88.
[39] Y. Q. Wu, F. L. Huang, Z. Y. Zhang, Experiments and modeling of hmx granular explosives subjected to drop-weight impact. *RSC Adv.* **2012**, *2*, 4152–4163.

Manuscript received: October 29, 2019
Revised manuscript received: March 2, 2020
Version of record online: May 14, 2020

